A Homology Model of the Pore Region of HCN Channels

A. Giorgetti, P. Carloni, P. Mistrik, and V. Torre
Istituto Nazionale per la Fisica della Materia (INFM-DEMOCRITOS Modeling Center for Research in Atomistic Simulation) and International School for Advanced Studies (SISSA), 34014 Trieste, Italy

ABSTRACT HCN channels are activated by membrane hyperpolarization and regulated by cyclic nucleotides, such as cyclic adenosine-mono-phosphate (cAMP). Here we present structural models of the pore region of these channels obtained by using homology modeling and validated against spatial constraints derived from electrophysiological experiments. For the construction of the models we make two major assumptions, justified by electrophysiological observations: i), in the closed state, the topology of the inner pore of HCN channels is similar to that of K^+ channels. In particular, the orientation of the S5 and S6 helices of HCN channels is very similar to that of the corresponding helices of the K^+ KcsA and K^+ KirBac1.1 channels. Thus, we use as templates the x-ray structure of these K^+ channels. ii), In the open state, the S6 helix is bent further than it is in the closed state, as suggested (but not proven) by experimental data. For this reason, the template of the open conformation is the x-ray structure of the MthK channel. The structural models of the closed state turn out to be consistent with all the available electrophysiological data. The model of the open state turned out to be consistent with all the available electrophysiological data in the filter region, including additional experimental data performed in this work. However, it required the introduction of an appropriate, experimentally derived constraint for the S6 helix. Our modeling provides a structural framework for understanding several functional properties of HCN channels: i), the cysteine ring at the inner mouth of the pore may act as a sensor of the intracellular oxidizing/reducing conditions; ii), the bending amplitude of the S6 helix upon gating appears to be significantly smaller than that found in MthK channels; iii), the reduced ionic selectivity of HCN channels, relative to that of K^+ channels, may be caused, at least in part, by the larger flexibility of the inner pore of HCN channels.

INTRODUCTION

HCN channels are members of the voltage-gated superfamily of ionic channels, regulated by cyclic nucleotides, such as cyclic adenosine-mono-phosphate (cAMP). In contrast to most Na^+ and K^+ ionic channels, which open when membrane potential is depolarized (1–7), they are opened when the membrane potential hyperpolarizes below ~ -50 mV.

HCN channels control fundamental biological events such as heart beat and neuronal rhythmic activity, providing the biophysical mechanism for the pacemaker (8–11) in these cells. These channels are composed of a cytoplasmic cAMP binding domain and a transmembrane domain. Although the x-ray crystal structure of the cytoplasmatic domain from the mouse channel has been determined recently (12) (mHCN2; Protein Data Bank accession number, 1Q3E), structural information on the pore domain is still lacking.

Indirect structural information has been inferred from experimental data on cloned channels, which have properties very similar to those of native HCN channels (13). These channels have been cloned from sea urchin sperm, referred to as spHCN (14,15) and from mammalian tissues, referred to as HCN1-4 (16–23). In particular, the HCN2 from *mouse* (mHCN2) has been experimentally widely investigated (1,24,25). Based on these data, it has been suggested that the pore regions of HCN share several important features with those of K^+ channels: i), in both families the pore domain includes four identical subunits (16), each featuring a loop forming the inner pore region together with an additional small helix (P-helix), not spanning the lipid membrane. The inner pore and the P-helix form the so-called P-helix-loop. Each subunit of voltage-gated K^+ channels and HCN channels features six transmembrane helices (referred to as S1-S6), whereas subunits of the KcsA and MthK K^+ channels have only two transmembrane helices (referred to as TM1-TM2), structurally similar to S5 and S6 in voltage-gated K^+ channels. S6 and TM2 are involved in gating, whereas the P-helix-loop does not change conformation upon gating (2,3,26). ii), The sequence of K^+ and HCN channels in the inner pore region is highly conserved and contains the GYG fingerprint, called the selectivity filter (27,28). Recently, this has been supported by an investigation of the pore topology of the spHCN channel (1). iii), Some of the structural features of the closed and open states are similar: In the closed state, the orientation of the S5 and S6 helices of HCN channels is very similar to that of the TM1 and TM2 helices of the KcsA channel (2). This suggestion is based primarily on the assumption that the great majority, if not all, of the ionic channels belonging to the superfamily of voltage-gated channels share the same molecular architecture and in particular the orientation in space of S5 and S6 helices (7). The open state of K^+ channels differs from the closed state only for the S6 helix (or TM2 helix in

Submitted May 3, 2004, and accepted for publication May 16, 2005.

Address reprint requests to V. Torre, E-mail: torre@sissa.it.

P. Mistrik's present address is University of Munich, Dept. of Pharmacy, Center for Drug Research, Munich 81377, Germany.

A. Giorgetti's present address is Biocomputing, Dept. of Biochemical Sciences, University of Rome 'La Sapienza', Rome, Italy.

0006-3495/05/08/932/13 $2.00

doi: 10.1529/biophysj.104.045286

the case of KcsA), which is bent toward the lipid phase, around a Gly residue that acts as gating hinge (29). This bending was indeed observed in the x-ray structure of the MthK (3) channel in the open state, and proposed to be a general feature. S6 in HCN channels is believed to exhibit a similar conformational change in the open state (6,30). This proposal is supported by the presence in this family of the Gly residue, which provides the gating hinge in K^+ channels, as well as of an Ala/Gly residue, five residues downstream in the so-called ''activation gate region'' (highlighted in *dark gray* in Fig. 1, *A* and *B*). This is further substantiated by electrophysiological experiments with wild-type (wt) and mutant spHCN channels (6,30).

Despite these similarities, the ion selectivity of HCN channel pore domains differ markedly from those of K^+ channels; the permeability ratio (P_{Na}/P_K) between Na^+ and K^+ ions in HCN channels ranges between 0.24 and 0.31 (16), whereas in K^+ channels the permeability ratio ranges between 0.18 and 0.03 (7,31). This indicates that HCN channels are less selective than K^+ channels and indeed, in physiological conditions, a current carried by a mixture of Na^+ and K^+ ions (usually referred to as I_h) flows through HCN channels (32–34).

Here we construct structural models of the HCN channels' pore region by homology modeling based on the available structural information on K^+ channels, exploiting the structural similarities between HCN and K^+ channels. Spatial constraints inferred by experimental data are then used to validate our models. We focus on the structures of spHCN (both in the closed and open states) and mHCN2 (in the closed state), as the pore region of these channels has been experimentally investigated (1,24,25). We explore a wide range of possible configurations, analyzing physical quantities that do not depend critically on the exact three-dimensional (3D) structure, but are likely to capture basic differences between K^+ and HCN channels, and, for the latter, between the closed and open states.

For the closed state, the templates could be in principle the available x-ray structures of the K^+ channels, namely the KcsA K^+ channel from *Streptomyces lividans* (2,26), the voltage gated K^+ channel from *Aeropyrum pernix* (KvAP) (4), and the inward rectifier K^+ channel from *Burkholderia pseudomallei* KirBac1.1 (5). However, as KvAP exhibits a wide-open conformation, thought to arise from crystal packing effects (4), only the other two structures were used.

Our model of the open state uses the MthK channel as a template (3,6).

The models are compared with structural constraints derived by electrophysiological experiments with wt and mutant channels reported previously (30) as well as with new experiments on Cd^{2+} blockage on spHCN and mHCN2 channels reported here. Models for the closed state derived from crystal structures are fully consistent with this data, however, those for the open state require the introduction of an appropriate constraint based on experimental data (30).

Based on our modeling, we provide a possible explanation for the different ionic selectivity between K^+ and HCN channels and suggest that the bending of the S6 helix upon gating is significantly smaller than that occurring in MthK channels.

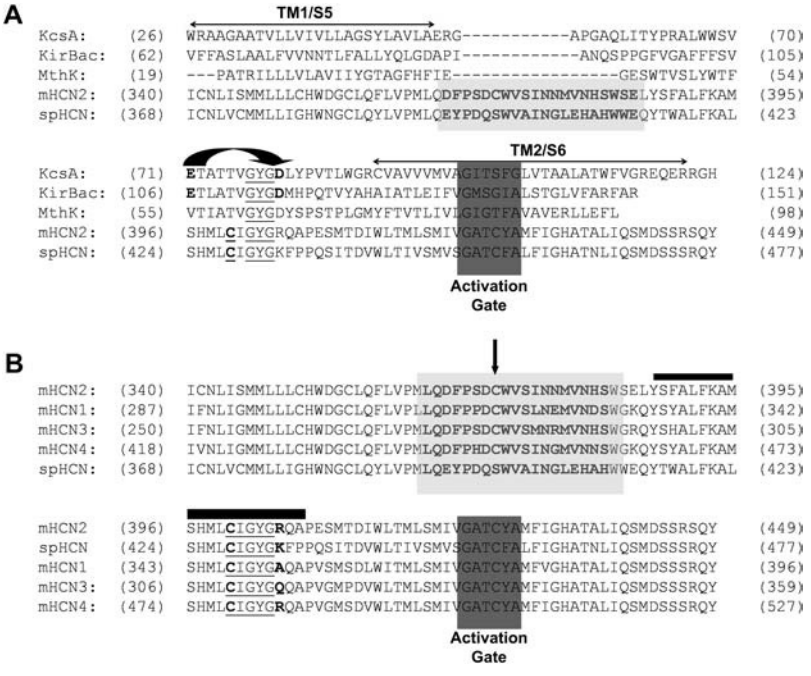

FIGURE 1 (*A*) Sequence alignment of pore regions of KcsA, KirBac1.1, MthK, mHCN2, and spHCN channels. The filter GYG fully conserved signature (16) is shown as underlined residues. The activation gate (29), highlighted in dark gray, begins with the fully conserved glycine residue acting as gating hinge and the Gly/Ala five residues downstream (29). In the KcsA channel, E71 and D80 (*bold* residues) form a very strong hydrogen bond. Such interaction is represented here with a curved arrow. The long extracellular loop present in spHCN and mHCN2 is highlighted in light gray. Double-headed arrows indicate location of TM1/S5 and TM2/S6. (*B*) Sequence alignment of pore regions of spHCN, mHCN1, mHCN2, mHCN3, and mHCN4 channels. The conserved residues in the inner pore region are underlined, whereas the residues present in the extracellular end of the inner pore are shown in bold. The activation gate in the S6 transmembrane helix and the large extracellular loop were highlighted in dark and light gray, respectively. The cysteine in the extracellular loop conserved in HCN1-4 channels, responsible for MTSES and MTSEA channel block (58), is marked with an arrow. A thick black line indicates the P-helix-loop, which comprises residues from Tyr-387 to Pro-408 (mHCN2). In panels *A* and *B*, HCN inner pore conserved Cys residue is represented with bold underlined fonts.

METHODS

Bioinformatics

Sequence alignment

The S5/S6 regions in the amino acid sequence of mHCN2 and spHCN channels were identified on the basis of the prediction of transmembrane helices, using the programs: DAS (http://www.biokemi.su.se/~server/DAS (35)); tmap, (http://www.embl-heidelberg.de/tmap/tmap_info.html (36,37)); PHDhtm (http://www.embl-heidelberg.de/predictprotein (38,39)); and TopPred2 (http://www.biokemi.su.se/~server/toppred2 (40)). The sequences including S5 and S6 turned out to be 368–477 in spHCN and 340–449 in mHCN2. The sequences of spHCN and mHCN2 channels were aligned with residues 26–124 of KcsA, 62–151 of KirBac1.1, and 19–98 of MthK, which correspond to the truncated sequence visible in the x-ray structures (2,3). The alignment was performed using the program ClustalW (41) (http://www2.ebi.ac.uk/clustalw). In the alignment, the following criteria were used: i), similarity of the P region (P-helix-loop) (1); ii), fully conservation of the G-Y-G motif in the filters (16,29); iii), alignment of S5 (spHCN) residues with TM1 in KcsA (2), KirBac1.1 (5), and MthK (3). iv), Alignment of S6 with TM2 in KcsA (2), KirBac1.1 (5), and MthK (3). Notice that a long gap (>11 residues) was inserted between the S5 and the pore-helix in the potassium channels to align the predicted transmembrane helices of the HCN channels with those of the templates.

Building of three-dimensional models

Three-dimensional models of the closed spHCN and mHCN2 and open spHCN were produced using Modeller 6v2 (42). The S5, S6, and the P-helix were restrained to adopt a helical conformation, and the noncrystallographic fourfold symmetry present in the KcsA, KirBac1.1, and MthK structures was enforced. The large extracellular loops, present in the two channels, have a very high variability and cannot be compared to existing regions in K^+ channels of known 3D structure. The best-scoring models were selected for each channel. These models provided also the best stereochemistry, as monitored by ProcheckV3.5 (43) and WhatifV4.99 (44) programs. Models of the channel in the closed state were consistent with all the available experimental data (see Results section). In contrast, the model of spHCN in the open state was not in agreement with the estimates of distances of opposing C_α along the S6 helix (30). In the open state, the analysis of Cd^{2+} blockage of mutant channels and of Cd^{2+} containing proteins (45,46) suggests that the distance between opposing C_α's for Thr-464 must be ~11 Å and ~14 Å for Glu-461, Asn-465, and Gln-468. These distances were not in agreement with those obtained using the MthK channel as a template (Table 1). Therefore, the MthK channel was used as a template, but with the constraint that the distance between opposing C_α's of Thr-464 should be ~11 Å. The experimental data on residues in positions 461, 465, and 468 were used for model validation.

TABLE 1 Distances of selected (opposite) C_α's along the S6 helix from spHCN structural models in the open and closed conformations

	Closed spHCN C_α distance (Å)	Open spHCN C_α distance (Å)	KcsA C_α distance (Å)	MthK C_α distance (Å)
Gly-461	9	13.3–13.5 (MD)	9.8 (A108)	23.7 (E92)
Thr-464	9	10.7–11 (MD)	9.5 (A111)	30.7 (L95)
Asn-465	11	15.1–15.5 (MD)	11.5 (T112)	29.3 (E96)
Gln-468	15	16.1–16.7 (MD)	10.9 (V115)	No data

In the open conformation, distances before and after the MD simulations (MD) are indicated. The distances for opposite Thr-464 in the open conformations were restrained to get agreement with experimental data. Distances corresponding to the homologous residues in the templates are also shown.

The domains were first inserted in a water/*n*-octane bilayer enclosed in a box of $\approx 77 \times 76 \times 83$ Å^3 (Fig. 1 in Supplementary Material), which was designed to mimic the cytoplasm/membrane environment (47,48). The portion of the protein immersed in the organic liquid spans for 34 Å from each membrane/water interfaces. Seven potassium counterions were added so as to insure electroneutrality of the systems. The structures were refined by energy minimization and a brief molecular dynamics (MD) run based on the AMBER 7.0 suite of programs (49). For the K^+, the force-field parameters derived by Aqvist (50) and adapted to the AMBER force field were used. The AMBER parm96 (51), TIP3P (52), and OPLS (53,54) force fields were used for the protein, water, and *n*-octane, respectively. The dielectric constant was set equal to 1. SHAKE algorithm was used to constrain all bonds (55). The time step was 0.0015 ps. Periodic boundary conditions were applied. The electrostatic interactions were treated using Ewald particle mesh methods (56) (using a grid spacing of ~1 Å^3). We used 10.0 Å as cutoff of the direct part of the Ewald sum and of the Lennard-Jones interactions. Geometry optimization was performed by the use of steepest descent (200 steps) and conjugate gradient algorithms (5000 steps). Constant temperature (300 K) and pressure (1 atm) MD simulations were achieved by using a Berendsen thermostat (coupling constant of 1 ps) and barostat (coupling constant 1 ps) (57). The geometry optimization was followed by a 1-ns MD simulation. MD simulations were performed on five different systems: KcsA, KcsA (E71V), spHCN (open and closed conformations), and mHCN2. These MD simulations are used only to sample the phase space.

Number of H-bonds

To estimate the rigidity/flexibility of HCN channels, relative to the KcsA channel, the number of H-bonds was counted. Counting H-bonds in KcsA is straightforward, but some care must be used when homology models are investigated. Therefore, several models for the spHCN, mHCN2, and mHCN3 channels were generated using Modeller6v2 (42) with different initial conditions, so to explore a variety of possible side-chain configurations. The different initial conditions were achieved by using different random numbers. Once models were generated, an H-bond count was carried out on the P-helix-loop from Tyr-415 to Pro-436 in spHCN, Tyr-387 to Pro-408 in mHCN2, and Tyr-297 to Pro-318 in mHCN3. All N-O and O-O atoms separated by a distance between 2.195 and 3.350 Å (following Swiss-Pdb Viewer protocols; http://www.expasy.org/spdbv) were considered as putative H donors and acceptors, respectively. The configuration space of possible models was sampled in the following way: for each channel 10 new models were generated using modeller6v2 and H-bonds were counted and listed. The procedure of model generation was stopped when for a new set of 10 different models no new H-bond distribution appeared. The procedure stopped after the generation of six groups of 10 different models.

Electrostatic potential along the channel axis

To estimate the electrostatic profile in the absence of a reliable 3D structure, a variety (see later) of 3D models of mHCN1, mHCN2, mHCN3, and spHCN channels were generated and the electrostatic potential profile was computed by solving the Coulomb equation along the channels' *z* axis. To take into account the presence of water molecules (different from ''bulk water'') in the cavity and in the inner pore region, a dielectric constant of 4 was used. Because far from the filter, water becomes ''bulk'', i.e., the dielectric constant increases, electrostatic profiles only in the neighborhoods of the inner pore were considered. Partial charges derived from the AMBER force field were used (51). The different 3D models for each of the HCN channels were generated by considering all possible rotamers of Arg-405 (for mHCN2), of Lys-433 (for spHCN), of Ala-352 (for mHCN1), and Gln-315 (for mHCN3). Rotamers were modeled by using Swiss-Pdb Viewer tools (http://www.expasy.org/spdbv) and the distribution was as follow: 18, 16, 6, and 2 different rotamer configurations for Arg, Lys, Gln, and Ala, respectively.

Experimental section

Molecular biology and expression in Xenopus *oocytes*

The spHCN channel from sea urchin sperm (14) and the HCN2 channel from mouse (mHCN2) (16) were subcloned in the pGEM-HE expression vector. cRNA (50 ng) was injected into *Xenopus laevis* oocytes. Stage IV-VI oocytes were surgically removed from female frogs anesthetized by immersion in 0.3% 3-aminobenzoic acid ethyl ester, followed by digestion with 1 mg/ml collagenase solution containing 88 mM NaCl, 1 mM KCl, 0.82 mM $MgSO_4$, 2.4 mM $NaHCO_3$, 5 mM TRIS (pH 7.4) for 60 min. Injected eggs were maintained at 18°C in a standard Barth solution supplemented with 50 μg/ml gentamycin sulfate and containing (in mM): 88 NaCl, 1 KCl, 0.82 $MgSO_4$, 0.33 $Ca(NO_3)_2$, 0.41 $CaCl_2$, 2.4 $NaHCO_3$, 5 TRIS, pH 7.4 (buffered with tetramethylammonium (TMAOH)). During the experiments, oocytes were kept in a Ringer solution containing (in mM): 150 NaCl, 2.5 KCl, 1 $CaCl_2$, 1.6 $MgCl_2$, 10 HEPES-TMAOH, pH 7.4 (buffered with TMAOH). All reagents were from Sigma Chemicals (St. Louis, MO).

Electrophysiological recordings

Cell-free inside-out patches were obtained 2–4 days after cRNA injection, and data were acquired using a patch-clamp amplifier (Axopatch 200B, Axon Instruments, Foster City, CA) at room temperature (20–22°C). Borosilicate glass pipettes had resistances of 3–5 MΩ in symmetrical standard solution. The solution in the patch pipette contained (in mM) 150 KCl, 10 HEPES, and 10 EGTA, buffered with TMAOH to appropriate pH 7.4. The solution bathing the intracellular side of the patch contained (in mM) 150 KCl, 10 HEPES, and appropriate amounts of $CdCl_2$. The intracellular bath solution was supplemented with 1 cAMP. Data were low-pass filtered at 1 kHz and acquired online at 5 kHz. Analysis was done using pClamp (Axon Instruments) and Origin software (Microcal Software, Northampton, MA). I_h currents were elicited by stepping the membrane voltage from 0 to -100 mV for 600 or 1400 ms for spHCN and mHCN2, respectively.

RESULTS

Here we first describe the structural features of the closed and open state of HCN channels, as obtained by homology modeling. Comparison is then made with experimental data reported in the literature and performed here.

Closed state

The amino acid sequence in the pore region (TM1/S5, P-helix-loop, and TM2/S6) of the KcsA, KirBac1.1, MthK, spHCN, and mHCN2 channels are aligned in Fig. 1 *A*. The overall sequence identity (SI) between targets and templates is low ($\approx$18% for all the templates). However, in the P-helix-loop (residues Tyr-415 to Pro-436 in spHCN and Tyr-387 to Pro-408 in mHCN2) SI increases significantly, and becomes $\sim$30% between targets and KcsA channel. The sequence alignment between K^+ and HCN channels requires the inclusion of a gap of $>$11 residues in KcsA, KirBac1.1, and MthK channel, between residues Gly-53 and Ala-54 (KcsA). In HCN channels, this region corresponds to a long extracellular loop (highlighted in *light gray* in Fig. 1 *A*) absent in K^+ channels.

Fig. 1 *B* illustrates the sequence alignment in the same region of the mHCN1, mHCN2, mHCN3, mHCN4, and spHCN channels. The overall SI is very high (of the order of 90%), but some significant differences are evident. In the inner pore region there is a cysteine conserved in all HCN channels (*bold underlined* cysteine residues in Fig. 1, *A* and *B*). According to the sequence alignment in Fig. 1 *A* and the 3D structure of the KcsA channel, these cysteines may form a ring at the intracellular mouth of the channel inner pore. The presence at the inner pore of a ring of cysteines able to oxidize and form disulfide bonds is a remarkable feature and some properties of these cysteines will be studied in spHCN and mHCN2 channels in the following sections. The inner pore region in HCN channels is composed of the residues C-I-G-Y-G-X, (in Fig. 1 *B*, CIGYG *underlined* residues; X residues shown in *bold*) where X can be positively charged, polar, or a neutral residue. X is a lysine in spHCN, an arginine in mHCN2 and mHCN4, but an alanine in mHCN1, and a glutamine in mHCN3. The S5 and S6 transmembrane helices are well conserved among the HCN channel family. In the activation gate region the motif GATCYA (highlighted in *dark gray* in Fig. 1 *B*) is fully conserved in HCN1-4 channels, but in the spHCN channel a tyrosine residue is replaced by a phenylalanine.

The large extracellular loop (highlighted in *light gray* in Fig. 1) has a similar sequence among HCN1-4 channels, but there are some differences between those and spHCN channel. For instance, in the middle of the loop there is a cysteine (indicated by a *gray arrow* in Fig. 1 *B*) conserved in all HCN channels, which is replaced by a serine in spHCN channels. This cysteine mediates the blockage of the I_h current by extracellular MTSEA and MTSES (58), indicating that the extracellular loop could approach the pore at a distance comparable to MTSEA length, i.e., $\sim$6 Å. As expected from a hydrophilic domain, residues forming the extracellular loops are polar and have a high probability for H-bond formation.

Models were constructed using homology modeling based on the sequence alignment shown in Fig.1 *A* (models are available at http://www.sissa.it/$\sim$giorget/pdb_files). Final models were refined by a 1-ns MD simulation (see Methods). As expected, the 3D architecture of the K^+ channels is maintained. The long loop regions are not shown because of the high variability and uncertainty of their location after using our modeling approach. The stereochemistry and quality of the final models, investigated with ProcheckV3.5 and WhatifV4.99 programs, validated the proposed models (Table 1 in Supplementary Material).

The inner pore

Homology models of the inner pore region of mHCN2 and spHCN channels are illustrated in Fig. 2, *A* and *B*, respectively. The C_α of residues (shown as *balls*) from His-397 to Arg-405 for the mHCN2 and from His-425 to Lys-433 for the spHCN channels are shown; in Fig. 2 *A*, a gray stick with a darker tip indicates the carbonyl groups. A marker of all known HCN channels is the presence of a cysteine residue two residues upstream of the filter motif GYG (Cys-428 for

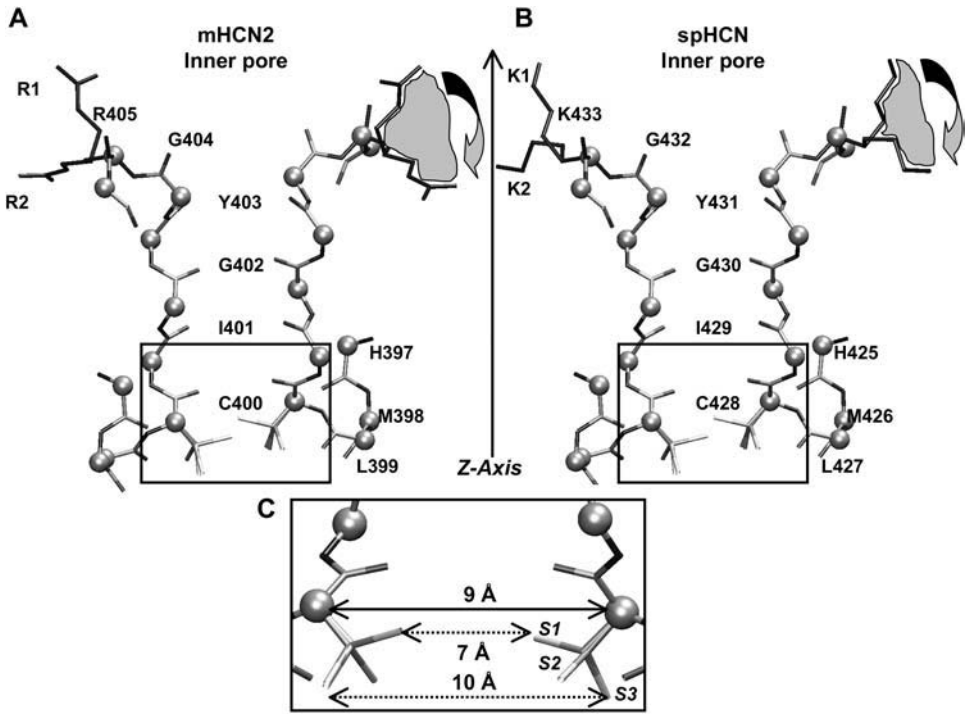

FIGURE 2 Homology model of the inner pore region of mHCN2 (*A*) and spHCN (*B*) channels in the closed state. Residues from His-397 to Arg-405, and from His-425 to Lys-433 are shown in panels *A* and *B*, respectively. The side chains of all residues except Arg-405 and Lys-433 are not shown. The rotamer space of Arg-405 and Lys-433 is shown as a shaded area: R1, R2 and K1, K2 indicate the extreme rotamers for Arg-405 and Lys-433, respectively. (*C*) Cysteine rotamer configurations for Cys-400 and Cys-428: S1, S2, and S3 indicate three different rotamer configurations. The homology model of the intracellular vestibule for mHCN2 and spHCN channels is the same. The solid line indicates the distance between C_α of opposing cysteines and the dotted lines indicate examples of distances between S atoms of opposing cysteines. Just two opposite subunits are shown.

spHCN and Cys-400 for mHCN2; see bold underlined cysteine in Fig. 1, *A* and *B*). Given the tetrameric structure of these channels, these cysteines form an intracellular ring (Fig. 2, *A* and *B*). In mHCN2 and spHCN channels at the outer mouth of the pore there is an arginine and a lysine, respectively, forming an extracellular ring of positive charges. The intracellular ring of cysteines and the extracellular ring of positive residues are key features of the inner pore of mHCN2 and spHCN channels.

Given the limitation of homology modeling it is difficult to determine the precise location of side chains and therefore we have investigated the configuration space of all possible rotamers of Arg-405 and Lys-433. These rotamers span wide angles centered on the corresponding C_α indicated by the shaded arrows in Fig. 2, *A* and *B*, respectively. The side chain of Arg-405 can point in the two extreme directions indicated by R1 and R2. Similarly the side chain of Lys-433 can point almost upward (see *K1*) and downward (see *K2*). MD simulations of the inner pore of these two channels show that the side chains of Arg-405 and Lys-433 move significantly and explore all the allowed rotamer configurations. These side chains do not seem to be anchored as the side chain of Asp-80 in the homologous position in the KcsA channel.

We now compare our structural models of the pore with electrophysiological experiments of Roncaglia and co-workers (1) and experiments performed here. These experiments are summarized in the next section.

Stoichiometry of intracellular Cd^{2+} blockage

Cd^{2+} ions usually bind in cysteine-containing proteins to two or more (up to four) S atoms. In addition, copper phenantroline (CuP) enhances the formation of disulfide bonds between two S atoms by oxidization. Because both agents experimentally block the current, at least two Cys residues must be able to bind Cd^{2+} ions and form S-S bridges.

Roncaglia et al. (1) have shown that Cys-428 of the spHCN channel mediates the blockage by intracellular Cd^{2+} of the wt spHCN channel. Roncaglia et al. have also shown that the mild oxidizing agent CuP added to the intracellular medium caused an irreversible blockage of the wt channel. Both Cd^{2+} and CuP blockage were significantly reduced in the mutant channel C428S where cysteine was replaced by serine. Cd^{2+} blockage of the I_h current flowing through wt spHCN channels described by Roncaglia et al. and by Rothberg et al. is different: Rothberg and co-workers (6) reported that 20 μM Cd^{2+} did not produce any blockage of the I_h current in wt spHCN channels, whereas Roncaglia and co-workers (1) described a significant blockage of the same current by 50 μM or more Cd^{2+} ions. To resolve this apparent discrepancy, the dose dependence of intracellular Cd^{2+} blockage, of spHCN and mHCN2 channels, was determined. Fig. 3, *A* and *B*, reproduce I_h currents recorded in the presence of different amounts of intracellular Cd^{2+} ions obtained from spHCN and mHCN2 channels expressed in *Xenous laevis* oocytes. Fig. 3 *C* shows the time course of Cd^{2+} blockage of the I_h current in the spHCN channel, when larger amounts of Cd^{2+} were added to the intracellular medium. The stoichiometry of intracellular Cd^{2+} blockage in the spHCN (*solid circles*) and mHCN2 (*open circles*) channels is shown in Fig. 3 *D*. The experimental results indicated that the residual I_h current flowing through spHCN channels in the presence of 20 μM intracellular Cd^{2+} was 57

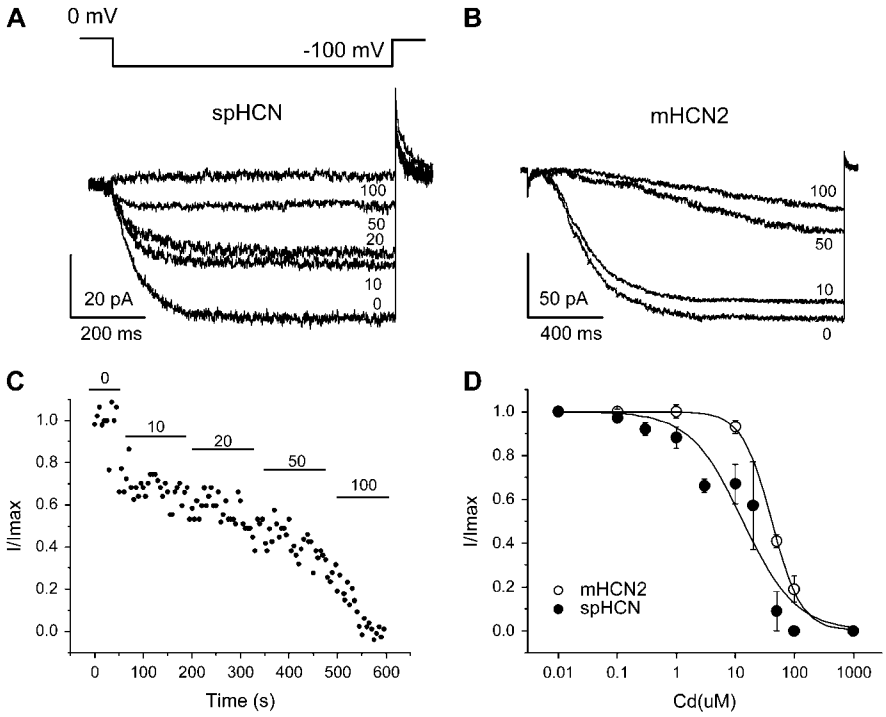

FIGURE 3 (*A* and *B*) The I_h current traces obtained in the presence of indicated micromolar concentrations of intracellular Cd^{2+} from the spHCN and mHCN2 channels, respectively. The I_h current was elucidated by hyperpolarizing the membrane patch in inside-out configuration from the holding potential of from 0 to −100 mV for 600 or 1400 ms for spHCN and mHCN2 channels, respectively. The traces are leak corrected. (*C*) Time course of the intracellular Cd^{2+} effect on the normalized amplitude of the I_h current from spHCN channel. The amplitude of current at a given Cd^{2+} concentration was determined from current traces like those in panel *A* by their normalization with respect to the amplitude in the absence of Cd^{2+}. (*D*) The dose dependence of the intracellular Cd^{2+} block of the spHCN and mHCN2 channels (●, ○, respectively). Data were fitted with the Hill function $I(c) = 1/(1 + (c/IC_{50})^N)$, where IC_{50} is the concentration necessary for the 50% block and N is the Hill coefficient. The best fitting was obtained with the values of $N = 1 \pm 0.2$ and $IC_{50} = 13 \pm 1$ μM for spHCN channel and $N = 1.7 \pm 0.1$ and $IC_{50} = 41.4 \pm 0.7$ μM for mHCN2 channel. Each experimental point represents mean ± SE from at least three experiments.

± 22%; as a consequence there is a partial blockage of the I_h current flowing through spHCN channels at the concentration used by Rothberg et al. (6). When a cysteine replaced Glu-461, Thr-464, Asn-465, and Gln-468, Rothberg et al. (6) reported a complete blockage of the I_h current by micromolar amounts of intracellular Cd^{2+}. In a more recent work, Rothberg and co-workers (59) probed intracellular Cd^{2+} effects on spHCN mutant channels L466C and Q468C at nanomolar concentrations. At these concentrations we never observed a blockage of the I_h in the wt channels.

The solid line through the experimental points was obtained with the Hill equation

$$I(c) = 1/(1 + (c/IC_{50})^N), \quad (1)$$

where c is the concentration of intracellular Cd^{2+}. A least-mean-square fitting of the experimental data provides values and $N = 1.7 \pm 0.1$ and $IC_{50} = 41.4 \pm 0.7$ μM for the mHCN2 channel. The fitting procedure provides instead a value of $N = 1 \pm 0.2$ and $IC_{50} = 13 \pm 1$ μM for the spHCN channel. This value of N, suggests that one Cd^{2+} ion is necessary to block the spHCN channel. Instead, the data for mHCN2 show that for larger concentrations of Cd^{2+}, the current traces seem not to be in equilibrium. Therefore, it may be appropriate to assume a noncooperative Cd-block in the pore.

In this respect, it is interesting to notice that Rothberg and co-workers (59) have fitted the experimental data of Cd^{2+} blockage on mutant channel Q468C with Eq. 1 using an N-value of 4 and IC_{50} of 72 nM. This result indicates that four Cd^{2+} ions block one mutant channel Q468C with a much higher affinity than the wt.

Comparison with experimental data

We now compare our models with the structural properties of the cysteine ring inferred by the electrophysiological experiments illustrated in Fig. 3 and in Roncaglia et al., 2002. Analysis of Cd^{2+} and Cys-containing protein structures performed by Krovetz et al. (45) and Giorgetti et al. (46), suggest that the range of most probable distances between the C_α for a pair of cysteines binding to Cd^{2+} falls between 4 and 9 Å (46,60,61) and between 4 and 7 Å for pairs of cysteines forming S-S bridges (46,62). Because the approximate diameter of Cd^{2+} is 1.8 Å and considering thermal fluctuations (63) the maximum distance $d(C_\alpha@Cys\text{-}C_\alpha@Cys)$ is expected to be of ~11 Å or less (45,46,60,61,64,65). In our models, $d(C_\alpha@Cys\text{-}C_\alpha@Cys)$ is ≈9 Å and ≈6.5 Å for opposite and adjacent cysteines, respectively, showing fully consistency with the experiments (Fig. 2 *A*). We have also investigated the configuration space of all possible rotamers of Cys-400 and Cys-428; three limiting rotamers were illustrated in Fig. 2 *C*. The S atom can point in several different directions: for some rotamers the distance of opposite S is 7 Å and for other rotamers 10 Å. In our models the expected distance for a Cd^{2+}-S interaction is ~2.5 Å. This distance is in agreement with that determined by x-ray diffraction between S atoms of cysteines forming the binding pocket for divalent cations (66,67).

Flexibility of the inner pore region

The 3D structure of the P-helix-loop of the proposed models of HCN channels in the close state is naturally very similar to that of the KcsA K^+ channel (residues from Tyr-62 to

Pro-83; see Fig. 4, *A* and *B*). However, the number of H-bonds with residues in the outer mouth of the channel decreases significantly on passing from the KcsA (26 H-bonds) to an average of 21.3 ± 1.5, 21.1 ± 1.4, and 21.1 ± 1.6 H-bonds for spHCN, mHCN2, and mHCN3 channels, respectively (shown as histograms in Fig. 4 *C*). We have generated 60 models for each of the pores of spHCN, mHCN2 (Fig. 4 *B*), and mHCN3 channels so as to include a wide range of side-chain configurations of the P-helix-loop. Residues from Tyr-415 to Pro-436 for spHCN and from Tyr-387 to Pro-408 in mHCN2 (indicated with a *black thick line* in Fig. 1 *B*) were considered. As shown in Fig. 4, *A* and *B*, the KcsA channel has more H-bonds (*dotted lines*) in the upper part of the inner pore. As a consequence, the inner pore of spHCN and mHCN2 channels is expected to be less rigid than that of K^+ channels. We provide further evidence of the different rigidity of the inner pore of these channels by calculating the β-factors based on MD simulations of KcsA, spHCN (closed conformation), and mHCN2 channels. To account for the presence of K^+ ions in the inner pore, three K^+ ions were located in the positions: S1, S3, and S_{cav} (68) (see Fig. 1 in Supplementary Material). Although positions S1 and S3 are not stable in MD simulations longer than 1 ns (68), it was known that substitution of Thr-75 (KcsA) with a cysteine increases the instability of S2-S4 configurations (69) and, as HCN channels have an endogenous cysteine in position corresponding to Thr-75 of the KcsA channel, it was decided to position K^+ ions only in S1 and S3. Fig. 5 shows that the fluctuations in the filter region are much larger in HCN channels than in the KcsA channel, confirming the different flexibility of the two families of ionic channels.

Is the number of H-bonds the only factor affecting the protein flexibility? To answer this question, we carried out also an MD simulation for the mutant E71V of the KcsA channel, which exhibits the same selectivity as the wt (70). The calculated β-factor of the mutant channel turns out to be very similar to that observed for the wt (Fig. 5). Thus, although the mutant has clearly a lower number of H-bonds at the pore region (namely 23 instead of 26) it does exhibit similar flexibility as wt. These results suggests that the larger flexibility of the pore region of HCN channels originates, at least in part, by the number of H-bonds and/or by the overall architecture of the protein scaffold, in a nontrivial manner.

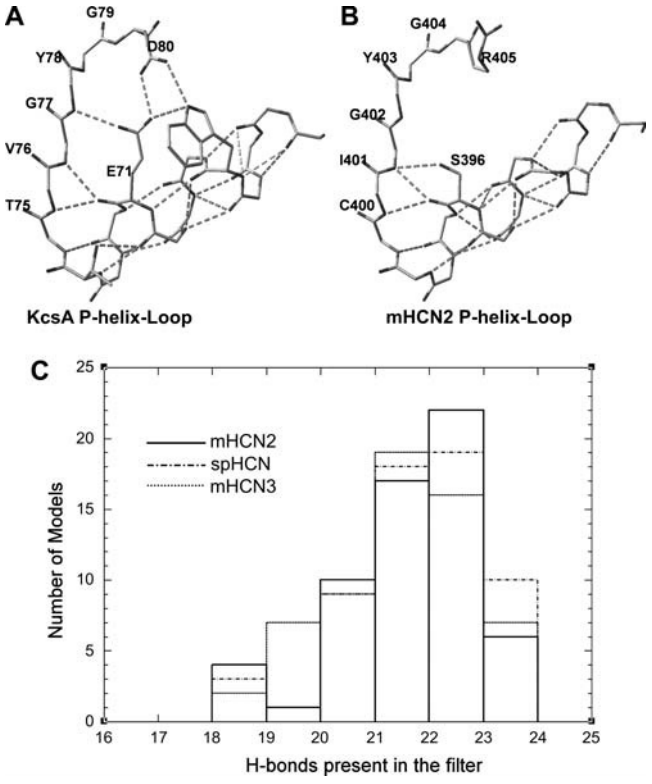

FIGURE 4 H-bond distribution in KcsA and mHCN2 channels in the P-helix-loop region (inner pore and P-helix), in the closed conformation. (*A*) Three-dimensional crystallographic structure of one subunit of the KcsA channel (2); (*B*) 3D model of one configuration of the mHCN2 channel. In panels *A* and *B* only side chains capable of H-bond formation are shown. H-bonds are indicated by dotted lines. The stabilizing H-bond network formed by Glu-71 and Asp-80 in the KcsA channel is absent in the HCN channels. (*C*) H-bond distribution for mHCN2 (*black*), for spHCN (*dotted-dashed*), and for mHCN3 (*dotted*) channels. The average number of H-bonds was 21.3 ± 1.5, 21.1 ± 1.4, and 21.1 ± 1.6 in the P-helix-loop region for spHCN, mHCN2, and mHCN3 channels, respectively. The configurations were obtained as described in the Methods section.

The electrostatic potential profile within the pore

As shown in Fig.1 *B* the inner pore of HCN channels is conserved (*underlined* residues) with the exception (*bold* residues) of the Lys-433 in spHCN, which becomes an

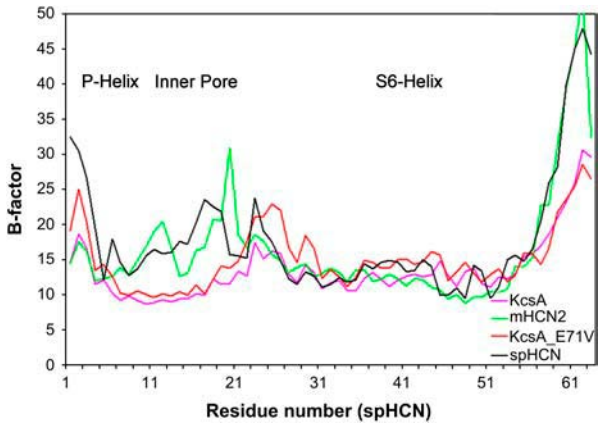

FIGURE 5 β-Factor of residues in the P-helix, the pore, and S6. Data obtained from 1-ns MD simulation for KcsA (*pink*), mHCN2 (*green*), spHCN (*black*), and KcsA E71V (*red*). Residue numbering corresponds to that of the spHCN channel (see the alignment in Fig. 1). The β-factor of the open and closed configuration of the spHCN channel superimpose and only data for the closed state are shown.

arginine in mHCN2 and mHCN4, an alanine in mHCN1, and a glutamine in mHCN3. The outer ring of positively charged residues in spHCN, mHCN2, and mHCN4 is expected to affect electrostatics in the pore and in the outer vestibule.

To estimate the electrostatic potential profile in the absence of a reliable 3D structure, a variety of 3D models of mHCN1, mHCN2, mHCN3, and spHCN channels were generated and for each of them the electrostatic profile along the pore axis was computed. All models had the same backbone, illustrated in Fig. 2, but differed in the direction of side chains of the outer ring of arginine, lysine, alanine, and glutamine. In Fig. 2, *A* and *B*, the allowed rotamers for Arg-405 and for Lys-433 are shown as shaded regions. The two extreme rotamers are marked *R1*, *R2* and *K1*, *K2*, respectively. As discussed in the Methods section for each HCN channel a family of electrostatic potential profiles was obtained.

Fig. 6 illustrates the electrostatic potential profile along the pore axis for different rotamers of the mHCN1, mHCN2, mHCN3, and spHCN channels. For HCN channels with an alanine or a glutamine the electrostatic potential profiles for the different rotamers are very similar, as expected from residues not bearing a net charge. As a consequence, the electrostatic potential profile for mHCN1 and mHCN3 channels is more negative near the extracellular vestibule than that of HCN channels with a positively charged ring, such as spHCN and mHCN2. The electrostatic potential profile for the mHCN2 and spHCN channels varies from ~−60 to −40 kcal/mol, according to the orientation of the side chain of the arginine or lysine. When side chains point toward the lipid phase (configurations *R2* and *K2* of Fig. 2 and corresponding potential profile in Fig. 6) the electrostatic potential profile is more negative than when side chains point upward and are almost parallel to the pore axis (configurations *R1* and *K1*).

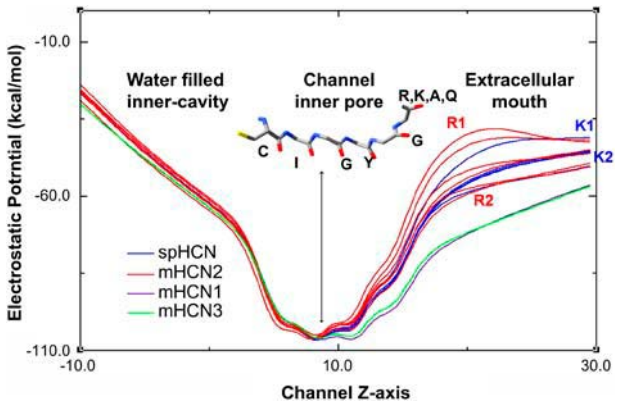

FIGURE 6 Electrostatic potential profile along the channel *z* axis for different rotamer configurations of mHCN2 (*red*), mHCN1 (*violet*), mHCN3 (*green*), and spHCN (*blue*) channels. The plot indicates the position of the different carbonyl oxygen from inner pore. The electrostatic profiles corresponding to the limiting rotamers—shown in Fig. 3—are labeled as *R1*, *R2* and *K1*, *K2*. Outside of the filter region the potential tends to zero (results not shown for clarity).

The open state

The spHCN channel is blocked by the compound ZD7288 (30) only in the open state. Shin and co-workers (30) have shown that three residues in the S6 region—Phe-456, Leu-458, and Ile-460—mediate the irreversible blockage of ZD7288. These residues are presumably located inside the cavity of the channel pore and the channel needs to open so that ZD7288 can bind to these residues. Upon channel closure the blocker could be trapped irreversibly inside the channel cavity. As a consequence an intracellular gate (6,30) involving conformational rearrangements of the S6 transmembrane helix as in K^+ channels (3) has also been proposed for HCN channels. To verify the existence of this gate and to identify the residues involved, cysteine scanning mutagenesis of the S6 transmembrane helix of spHCN channels was used (Rothberg et al., 2002). When Thr-464 was mutated into a cysteine, small amounts of intracellular Cd^{2+} produced an irreversible blockage of the mutant channel, likely to be caused by the coordination of three or more S atoms with a Cd^{2+} ion. As a consequence the distance between opposing C_α of these exogenous cysteines is expected to be of ~11 Å. When Gly-461 and Asn-465 were mutated into a cysteine, Cd^{2+} ions powerfully blocked mutant channels G461C and N465C in the open state. Cd^{2+} blockage of mutant channels G461C, T464C, N465C, and Q468C in the open state are not in agreement with a model of the spHCN channel using the MthK channel as a template (see Fig. 7 *A* and Table 1). Therefore, the extent of bending of the S6 helix, upon gating, in K^+ and HCN channels may be different. As discussed in the Methods section, to obtain a realistic model of the spHCN channel in the open state, the MthK channel was used as a template but with the additional constraint that the distance between opposite Thr-464 be ≈11 Å.

Fig. 7 *A* reproduces the templates used for our homology modeling for the open (MthK channel in *red*) and closed (KcsA channel in *blue*) channel. Fig. 7 *B* illustrates the final models of the spHCN channels in the open (*red*) and closed state (*blue*). The bending of the S6 transmembrane helix associated to gating in K^+ channels is ≈30° whereas in our model of spHCN channels, this angle decreases to ~12°. Rothberg et al. (59) have shown that the mutant channel Q468C of the spHCN channel is blocked in the closed state very powerfully by Cd^{2+} ions with an affinity of 72 nM suggesting the simultaneous binding of four Cd^{2+} ions. The proposed model of the pore of the spHCN channel in the closed state is compatible with the proposed Cd^{2+} blockage. In our model the distance between opposite C_α of exogenous cysteines in the mutant channel is ≈15 Å so that it may be possible to accommodate among neighboring S a Cd^{2+} ion and obtain the proposed configuration S-Cd-S-Cd-S-Cd-S-Cd (66,67).

To test the stability of the proposed model, 1-ns MD simulations were performed for spHCN model in the open pore configuration (see Methods). Fig. 7 *C* shows the initial

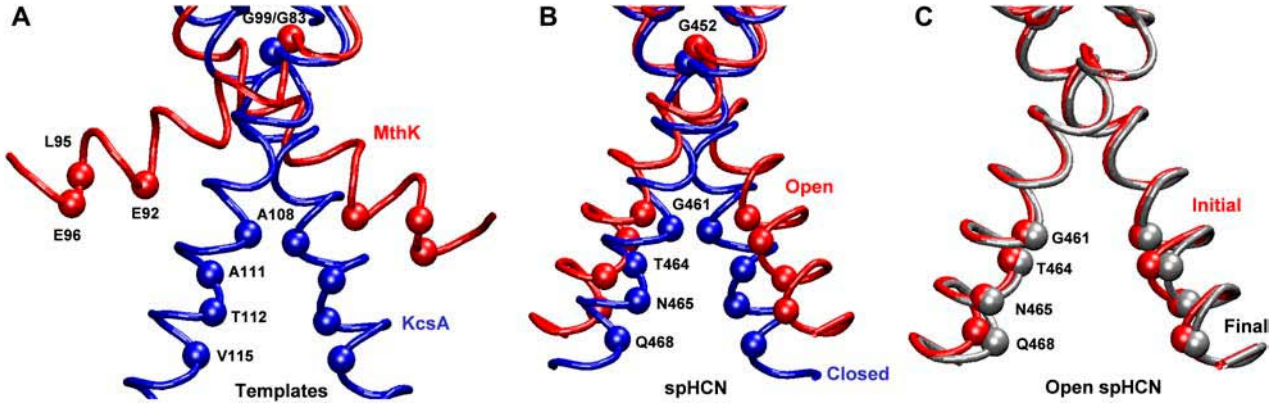

FIGURE 7 The open (*red*) and closed (*blue*) channel conformations. (*A*) Templates used for homology modeling for the open (MthK channel in *red*) and closed (KcsA channel in *blue*) channel. (*B*) Final models of the spHCN channels in the open (*red*) and closed state (*blue*). (*C*) Superimposition of the initial (*red*) and final (*gray*) MD simulation snapshots (open configuration of the spHCN channel). The bending of the S6 transmembrane helix associated with gating in K^+ channels is ≈30° whereas in our model of spHCN channels the bending is ≈12°. Only two subunits are shown. Selected residues are shown as spheres. Distances between opposite C_α–C_α atoms obtained from the modeling are compared with estimates from experimental data in Table 1.

(*red*) and the final (*gray*) structures superimposed; the overall root-mean-square deviation was ~1.8 Å, indicating that the model was stable. The displacements between the initial and the final configurations for selected atoms are shown in Table 1. A comment on the structure of the pore filter in the open state is necessary. The functional properties of HCN and spHCN channels are intermediate between those of K^+ and CNG channels. However, the filters of these channels exhibit very different properties: the filter of K^+ channels does not have major conformational changes during gating (with the exception of molecular events related to C-type inactivation (29)), whereas that of CNG channels does rearrange upon gating (71–73). Thus, we can draw no conclusions on the structure of the pore obtained by MD simulation, albeit this structure is stable in the timescale investigated.

Fig. 8 reproduces the proposed molecular structure around the gate located between Thr-464 and Gln-468 in the closed (*A*) and open state (*B*). The Connolly surface, in gray, obtained using the VMD1.8.2 program (http://www.ks.uiuc.edu/research/vmd/) with a probe radius of 0.90 Å, indicates the accessible free space. It is evident that the gate is closed in panel *A* whereas it is open in panel *B*.

As shown in Fig. 8, the gate in spHCN channels seems to be located near Gln-468, in agreement with the experimental observation that mutant channel T464C is not blocked by Cd^{2+} ions in the closed state but only in the open state (6). On the contrary the mutant channel Q468C is powerfully blocked by Cd^{2+} ions also in the closed state, suggesting that Gln-468 is accessible from the intracellular side of the membrane also in the closed state (59). Fig. 8 *C* illustrates our model of the open channel configuration of the mutant T464C, where the distance between C_α of opposing exogenous cysteines is ≈11 Å, so that one Cd^{2+} ion can bound to multiple cysteines (6). Cd^{2+} blockage of the mutant channel Q468C of the spHCN (59) is different: indeed, Cd^{2+} ions block the mutant channel in the closed state with four Cd^{2+} ions blocking one channel. Fig. 8 *D* illustrates our model of the mutant channel Q468C in the closed state: distances between C_α of opposing exogenous cysteines are ~15 Å, therefore allowing the coordination of four Cd^{2+} ions, as shown in Fig. 8 *D*.

DISCUSSION

We have constructed the structural models of spHCN and mHCN2 channels' transmembrane domains in the closed state, and that of spHCN in the open state. These models were obtained by homology modeling using the crystal

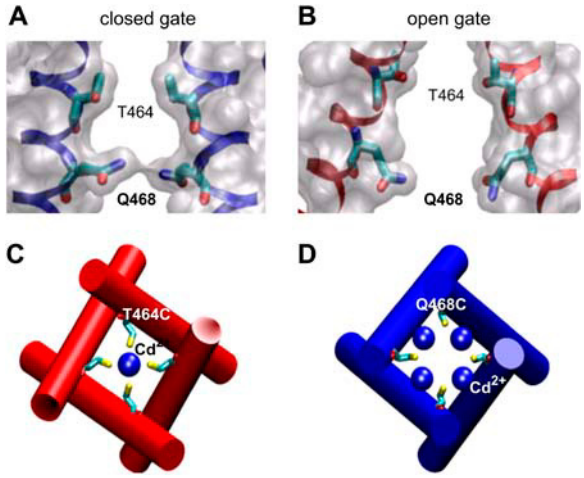

FIGURE 8 (*A* and *B*) The gate of the spHCN channel in the open and closed configuration, respectively. In gray is the Connolly surface obtained using the VMD1.8.2 program (http://www.ks.uiuc.edu/research/vmd/) with a probe radius of 0.90 Å. (*C*) Cd^{2+} block in mutant channel T464C in the open state. Distances between C_α of opposite cysteines in the open state were ≈11 Å. (*D*) Cd^{2+} block in mutant channel Q468C in the closed state. Distances between C_α of opposite cysteines in the closed state were ≈15 Å.

structure of the KcsA channel (2) and KirBac1.1 (5) as templates for the closed conformation and the MhtK channel (3) for the open conformation, using the assumptions outlined in the Introduction. In this section, we discuss insights on structure/function relationships in HCN channels based on the proposed models.

The closed state

The closed state models of spHCN and mHCN2 were validated against structural constraints inferred by experimental data available in the literature (1). The models were found to be consistent with all of the data. This supports the use of the models for investigation of structure features of the filter, the P-helix, and S6.

Flexibility of the inner pore and ion selectivity

The great majority of HCN and K^+ channels share the GYG motif in the pore. The ionic selectivity of these channels, however, is different: K^+ channels are primarily permeable for K^+ and Rb^+ ions and the permeability ratio P_{Na}/P_K is below 0.1. On the contrary, a distinct feature of all HCN channels is a significant permeability also to Na^+ ions, with $P_{Na}/P_K \sim 0.3$.

Here we argue that the lower selectivity of HCN channels relative to that of K^+ channels can be ascribed, at least in part, to the different flexibility of the selectivity filter, which is one of the primary determinants of ionic selectivity (31). In this view, K^+ channels have a radius of $\sim$1.5 Å, large enough for the permeation of alternating, single-file K^+ ions and water molecules, as confirmed by high-resolution x-ray crystallography (2). In HCN, the inner pore is relatively flexible, as suggested by a calculation of β-factors based on MD simulations on these channels (Fig. 5). Thus, partly hydrated Na^+ ions will be able to permeate through the selectivity filter. If, instead, the inner pore is less flexible, as is the case for the KcsA channel (Fig. 5), Na^+ ions, with several water molecules attached (74) will not be able to pass and the channel will be highly selective for K^+ ions. In turn, the larger flexibility of HCN channels could be ascribed, in part, to the smaller number of H-bonds in the P-helix and the inner pore region in the HCN channels relative to the K^+ channel (Fig. 4). However, this cannot be the only key factor for flexibility as shown by an additional simulation on the E71V K^+ channel mutant, which exhibits a lower number of H-bonds relative to wt and yet similar flexibility (Fig. 5) and permeability ratio (70) as wt. Thus, results from ''static'' crystal structures (H-bond) do not necessarily allow predictions about origin and determinants of protein flexibility or rigidity, as has been pointed out very recently by Allen et al. (75).

The cysteine rings

All HCN channels bear a cysteine in the inner pore region, as shown in Fig. 1 *B* (*bold underlined* Cys). Cd^{2+} ions from the cytoplasmic side of the membrane block spHCN and mHCN2 channels with an IC_{50} of 13 $\pm$ 1 and 41.4 $\pm$ 0.7 μM, for spHCN and mHCN2 channels, respectively (see Fig. 3). These results show that these cysteines are located at the intracellular side of the inner pore and form the cytoplasmic vestibule (1).

In CNGA1 channels from bovine rods, Cys-428 of spHCN channels is replaced by a threonine. When this threonine is replaced by a cysteine, the resulting mutant channel, T360C, is blocked by intracellular Cd^{2+} ions in the open state with an IC_{50} of $\sim$25 μM and a value of $N = 2$ (M. Mazzolini, A. V. Nair, A. Giorgetti, and V. Torre, unpublished data). Therefore, the cysteine ring (Fig. 2 *B*) in the inner pore region of HCN channels and of mutant channels T360C of CNGA1 from bovine rods is likely to have a similar molecular arrangement.

One Cd^{2+} ion is bound at least to three cysteines in the pore of the mutant channel T464C in the open state (6). As a consequence one Cd^{2+} is likely to coordinate to the four exogenous cysteines of mutant T464C, as shown in Fig.8 *C*. Cd^{2+} blockage of the mutant channel Q468C of the spHCN (59) is different: indeed, these authors have fitted the experimental data with Eq. 1, but with an *N*-value of 4 and an IC_{50} value of 72 nM. This result indicates that four Cd^{2+} ions block one mutant channel with a much higher affinity. The physical arrangement of Cd^{2+} ions and of the cysteines is illustrated in Fig. 8 *D*.

It is useful to stress the different blockage by Cd^{2+} ions in the pore of spHCN and CNGA1 channels and in the channel mutant Q468C; Cd^{2+} blockage in mutant T360C of the CNGA1 channel and in the pore of the spHCN channel (see Fig. 3) occurs presumably because the Cd^{2+} ions physically occlude the pore, whereas blockage of the mutant Q468C of the spHCN channel is of the lock-closed type in which the channel becomes locked in the closed configuration.

Under normal conditions HCN channels are open and therefore these cysteines do not form S-S bonds. The distance between opposite C_αs of these cysteines is $\approx$9 Å, suggesting that S-S bridges can be readily formed in the presence of an oxidizing medium. As a consequence, the inner pore of HCN channels is likely to be a sensor of the intracellular oxidizing/reducing conditions. Given the limitation of homology modeling it is very difficult and almost impossible to provide an explanation why Cd^{2+} ions bind with different affinities the ring of the native Cys-428 and of exogenous cysteines introduced in position 464 or 468.

The pore electrostatics

As shown in Fig. 6 the electrostatic potential profile obtained from our modeling is slightly different for the various HCN channels. In agreement with the K^+ pore structure the carbonyl groups of the signature GYG point toward the pore axis and provide an attracting binding site for cations. The computed electrostatic potential profile in the outer part of

the pore is more negative for mHCN1 and mHCN3 channels. Given the positive charge of Arg and Lys present in the outer mouth of mHCN2, mHCN4, and spHCN channels the electrostatic potential profile for all considered rotamers was consistently less negative than for mHCN1 and mHCN3. Therefore, differences of single-channel properties conductance among HCN channels could be expected. Given the small single channel conductance of HCN channels(1,6,30) it may be difficult to experimentally establish these differences.

The open state

As the homology model-based structure of the spHCN channel in the open state is not consistent with the available experimental data in the S6 helix, it has been refined by introducing experimentally derived constraints, which involve residues present in the S6 helix. Notice that the constraints between the C_α's belonging to opposite T464 are not consistent with the MhtK-based homology model of the channel, even including the fact that the channel may fluctuate between the open state (modeled based on the MthK channel) and the closed state (modeled based on the KcsA channel). Indeed, to satisfy such constraints one should suppose that the channel spends as much as 90% of its time in the closed state in the presence of cyclic nucleotides. Here we discuss structural features of S6 helices, for which comparison is made with the correspondent structural elements in K^+ channels.

The transition between the closed and open state in bacterial K^+ channels is associated with a significant bending of the S6 transmembrane helix around a hinge located around a conserved glycine (see Fig. 1 *A*). This bending in bacterial K^+ channels is associated with an angular rotation of ~30° around the hinge (3,29). The gating in spHCN channels seems to occur by similar mechanisms (6), but with a smaller rotation of ~12°. As shown in Fig. 8, the gate in spHCN channels seem to be located near Gln-468: indeed the mutant channel T464C is blocked by Cd^{2+} ions only in the open state, suggesting that Thr-464 is accessible from the intracellular side only in the open state (6). On the contrary the mutant channel Q468C is powerfully blocked by Cd^{2+} ions also in the closed state and therefore Gln-468 is accessible from the intracellular side of the membrane also in the closed state (59). At the speculative level, we anticipate that the gating in the large superfamily of voltage-gated ionic channels is likely to be caused by a movement of the S6 transmembrane helix, but its extent and properties are likely to depend on the specific ionic channel.

We close this section by using our model to provide a rationale for current measurements on adducts between spHCN mutant channels and Cd^{2+}, which shows that: i), submicromolar quantities of Cd^{2+} ions greatly slow down closure of L466C, once opened at negative voltages (59).

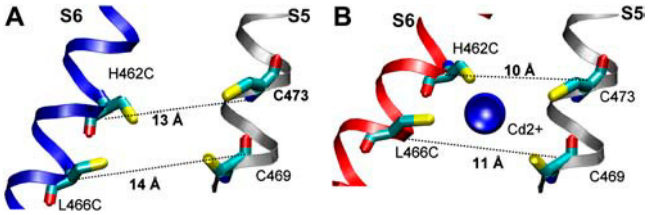

FIGURE 9 Proposed mechanism of Cd^{2+} binding to the double mutant H462C-L466C. (*A*) In the closed state, the distance between C_α @Cys-462 and C_α@Cys-473, located on S5, is ~13 Å, whereas and the distance between C_α@Cys-466 and C_α@Cys-469 in S5 is ~14 Å and, therefore, too large for Cd^{2+} ion binding. (*B*) In the open state, these two distances are reduced to ~10 and 11 Å, respectively, so that one Cd^{2+} ion can bind and lock the channel.

ii), In the presence of Cd^{2+} ions, the double mutant channel H462C-L466C once opened remains locked in the open configuration.

In our model, residues His-462 and Leu-466 do not point toward the channel axis and instead face toward other channel domains, such as S5. The spHCN channel has two native cysteines, Cys-473 and Cys-469 in S5, which according to our homology model are approximately at the same height of His-462 and Leu-466 in S6. Because S6 is relatively far in the closed state, the distance between His-462 and Cys-473 is as large as ≈13 Å and that between Leu-466 and Cys-469 ≈14 Å. Therefore, in the closed state there is no binding site for Cd^{2+} ions in mutant channel H462C-L466C, as shown in Fig. 9 *A*. In the open state, these distances become shorter and approach values between 10 and 11 Å so that one Cd^{2+} ion can tightly bind to cysteines in position 462, 466, 473, and 469, stabilizing, therefore, the open channel configuration, as shown in Fig. 9 *B*.

For CNGA1 channels, Cd^{2+} may also stabilize the open channel configuration in some cysteine mutant channels by a similar mechanism (A. V. Nair, M. Mazzolini, P. Codega, A. Georgetti, and V. Torre, unpublished data). Indeed, Cd^{2+} ions and CuP stabilize the mutant channel F380C in the open state, but this effect is not observed in the double mutant F380C-C314S, i.e., when the endogenous Cys-314 in the S5 is mutated to a serine.

SUPPLEMENTARY MATERIAL

An online supplement to this article can be found by visiting BJ Online at http://www.biophysj.org.

We thank Anna Tramontano for her comments on the article and Iain McLay for very useful discussions.

We thank GlaxoSmithKline for financial support. This work was also supported by a Human Frontier Science Program grant (RGP0054/2002) to V.T., and a grant from the Regione Friuli Venezia Giulia and CIPE (GRAND).

REFERENCES

1. Roncaglia, P., P. Mistrik, and V. Torre. 2002. Pore topology of the hyperpolarization-activated cyclic nucleotide-gated channel from sea urchin sperm. *Biophys. J.* 83:1953–1964.
2. Zhou, Y., J. H. Morais-Cabral, A. Kaufman, and R. MacKinnon. 2001. Chemistry of ion coordination and hydration revealed by a K+ channel-Fab complex at 2.0 A resolution. *Nature.* 414:43–48.
3. Jiang, Y., A. Lee, J. Chen, M. Cadene, B. T. Chait, and R. MacKinnon. 2002. Crystal structure and mechanism of a calcium-gated potassium channel. *Nature.* 417:515–522.
4. Jiang, Y., A. Lee, J. Chen, V. Ruta, M. Cadene, B. T. Chait, and R. MacKinnon. 2003. X-ray structure of a voltage-dependent K+ channel. *Nature.* 423:33–41.
5. Kuo, A., J. M. Gulbis, J. Antcliff, T. Rahman, E. Lowe, J. Zimmer, J. Cuthbertson, F. M. Ashcroft, T. Ezaki, and D. A. Doyle. 2003. Crystal structure of the potassium channel KirBac1.1 in the closed state. *Science.* 3000:1922–1926.
6. Rothberg, B., K. Shin, P. Phale, and G. Yellen. 2002. Voltage-controlled gating at the intracellular entrance to a hyperpolarization-activated cation channel. *J. Gen. Physiol.* 119:83–91.
7. Hille, B. 2001. Ionic Channels of Excitable Membranes, 3rd Ed. Sunderland, MA.
8. Halliwell, J., and P. Adams. 1982. Voltage-clamp analysis of muscarinic excitation in hippocampal neurons. *Brain Res.* 250:71–92.
9. DiFrancesco, D. 1993. Pacemaker mechanisms in cardiac tissues. *Annu. Rev. Physiol.* 55:455–472.
10. Brown, H., and W. Ho. 1996. *In* Molecular Physiology and Pharmacology of Cardiac Ion Channels and Transporters. M. Morad, S. Ebashi, W. Trautwein, and Y. Kuraki, editors. Kluwer, Dordrecht, The Netherlands.
11. Pape, H. 1996. Queer current and pacemaker: the hyperpolarization-activated cation currents in neurons. *Annu. Rev. Physiol.* 58:299–327.
12. Zagotta, W. N., N. Olivier, K. Black, E. Young, R. Olson, and E. Gouaux. 2003. Structural basis for modulation and agonist specificity of HCN pacemakers channels. *Nature.* 425:200–205.
13. Moroni, A., L. Gorza, M. Beltrame, B. Gravante, T. Vaccari, M. Bianchi, C. Altomare, R. Longhi, C. Heurteaux, M. Vitadello, A. Malgaroli, and D. DiFrancesco. 2001. Hyperpolarization-activated cyclic nucleotide-gated channel 1 is a molecular determinant of the cardiac pacemaker current I(f). *J. Biol. Chem.* 276:29233–29241.
14. Gauss, R., R. Seifert, and U. B. Kaupp. 1998. Molecular identification of a hyperpolarization-activated channel in sea urchin sperm. *Nature.* 393:583–587.
15. Robinson, R., and S. Siegelbaum. 2003. Hyperpolarization-activated cation currents: from molecules to physiological function. *Annu. Rev. Physiol.* 65:453–480.
16. Ludwig, A., X. Zong, M. Jeglitsch, F. Hofmann, and M. Biel. 1998. A family of hyperpolarization-activated mammalian cation channels. *Nature.* 393:587–591.
17. Ludwig, A., X. Zong, J. Stieber, R. Hullin, and F. Hofmann. 1999. Two pacemaker channels from human heart with profoundly different activation kinetics. *EMBO J.* 18:2323–2329.
18. Santoro, B., D. Liu, H. Yao, D. Bartsch, E. Kandel, S. Siegelbaum, and G. Tibbs. 1998. Identification of a gene encoding a hyperpolarization-activated pacemaker channel of brain. *Cell.* 93:717–729.
19. Santoro, B., and G. Tibs. 1999. The HCN gene family: molecular basis of the hyperpolarization-activated pacemaker channels. *Ann. N. Y. Acad. Sci.* 868:714–764.
20. Seifert, R., A. Scholten, R. Gauss, A. Mincheva, P. Lichter, and U. B. Kaupp. 1999. Molecular characterization of a slowly gating human hyperpolarization-activated channel predominantly expressed in thalamus, heart and testis. *Proc. Natl. Acad. Sci. USA.* 868:741–764.
21. Vaccari, T., A. Moroni, M. Rocchi, L. Gorza, M. Bianchi, M. Beltrame, and D. DiFrancesco. 1999. The human gene coding for HCN2, a pacemaker channel of the heart. *Biochim. Biophys. Acta.* 1446:419–425.
22. Shi, W., R. Wymore, H. Yu, J. Wu, R. Wymore, Z. Pan, R. Robinson, J. Dixon, D. McKinnon, and I. Cohen. 1999. Distribution and prevalence of hyperpolarization-activated cation channel (HCN) mRNA expression in cardiac tissues. *Circ. Res.* 85:1–16.
23. Ishii, T., M. Takano, L. Xie, A. Noma, and H. Ohmori. 1999. Molecular characterization of the hyperpolarization-activated cation channel in rabbit heart sinoatrial node. *J. Biol. Chem.* 274:12835–12839.
24. Azene, E., T. Xue, and R. Li. 2003. Molecular basis of the effect of potassium on heterologously expressed pacemaker (HCN) channels. *J. Physiol.* 547:349–356.
25. Xue, T., E. Marban, and R. Li. 2002. Dominant-negative suppression of HCN1- and HCN2-encoded pacemaker currents by an engineered HCN1 construct: insights into structure-function relationships and multimerization. *Circ. Res.* 90:1267–1273.
26. Doyle, D. A., C. J. Morais, R. A. Pfuetzner, A. Kuo, J. M. Gulbis, S. L. Cohen, B. T. Chait, and R. MacKinnon. 1998. The structure of the potassium channel: molecular basis of K+ conduction and selectivity. *Science.* 280:69–77.
27. Heginbotham, L., T. Abramson, and R. MacKinnon. 1992. A functional connection between the pores of distantly related ion channels as revealed by mutant K+ channels. *Science.* 258:1152–1155.
28. Heginbotham, L., Z. Lu, T. Abramson, and R. MacKinnon. 1994. Mutations in the K+ channel signature sequence. *Biophys. J.* 66:1061–1067.
29. Jiang, Y., A. Lee, J. Chen, M. Cadene, B. T. Chait, and R. MacKinnon. 2002. The open pore conformation of potassium channels. *Nature.* 417:523–526.
30. Shin, K., B. Rothberg, and G. Yellen. 2001. Blocker state dependence and trapping in hyperpolarization-activated cation channels: evidence for an intracellular activation gate. *J. Gen. Physiol.* 117:91–101.
31. Laio, A., and V. Torre. 1999. Physical origin of selectivity in ionic channels of biological membranes. *Biophys. J.* 76:129–148.
32. Clapham, D. 1998. Not so funny anymore: pacing channels are cloned. *Neuron.* 21:5–7.
33. Wollmuth, L., and B. Hille. 1992. Ionic selectivity of Ih channels of rod photoreceptors in tiger salamanders. *J. Gen. Physiol.* 100:749–765.
34. Ho, W., H. Brown, and D. Noble. 1994. High selectivity of the If channels to Na+ and K+ in rabbit isolated sinoatrial node cells. *Pflugers Arch.* 426:68–74.
35. Cserzo, M., E. Wallin, I. Simon, G. von Heijne, and A. Elofsson. 1997. Prediction of transmembrane alpha-helices in prokaryotic membrane proteins: the dense alignment surface method. *Protein Eng.* 10:673–676.
36. Persson, B., and P. Argos. 1994. Prediction of transmembrane segments in proteins utilising multiple sequence alignments. *J. Mol. Biol.* 237:182–192.
37. Persson, B., and P. Argos. 1997. Prediction of membrane protein topology utilizing multiple sequence alignments. *J. Protein Chem.* 16: 453–457.
38. Rost, B., R. Casadio, P. Fariselli, and C. Sander. 1995. Transmembrane helices predicted at 95% accuracy. *Protein Sci.* 4:521–533.
39. Rost, B. 2001. Review: protein secondary structure prediction continues to rise. *J. Struct. Biol.* 134:204–218.
40. von Heijne, G. 1992. Membrane protein structure prediction. Hydrophobicity analysis and the positive-inside rule. *J. Mol. Biol.* 225:487–494.
41. Thompson, J. D., D. G. Higgins, and T. J. Gibson. 1994. CLUSTAL W: improving the sensitivity of progressive multiple sequence alignment through sequence weighting, position-specific gap penalties and weight matrix choice. *Nucleic Acids Res.* 22:4673–4680.
42. Sanchez, R., and A. Sali. 1997. Advances in comparative protein-structure modelling. *Curr. Opin. Struct. Biol.* 7:206–214.

43. Laskowski, R. A., J. A. Rullmannn, M. W. MacArthur, R. Kaptein, and J. M. Thornton. 1996. AQUA and PROCHECK-NMR: programs for checking the quality of protein structures solved by NMR. *J. Biomol. NMR.* 8:477–486.

44. Vriend, G. 1990. WHAT IF: a molecular modeling and drug design program. *J. Mol. Graph.* 8:52–56.

45. Krovetz, H., H. VanDongen, and A. VanDongen. 1997. Atomic distance estimates from disulfides and high-affinity metal-binding sites in a K channel pore. *Biophys. J.* 72:117–126.

46. Giorgetti, A., A. V. Nair, P. Codega, V. Torre, and P. Carloni. 2005. Structural basis of gating of CNG channels. *FEBS Lett.* 579:1968–1972.

47. Moore, P. B., Q. Zhong, T. Husslein, and M. L. Klein. 1998. Simulation of the HIV-1 Vpu transmembrane domain as a pentameric bundle. *FEBS Lett.* 431:143–148.

48. Zhong, Q., T. Husslein, P. B. Moore, D. M. Newns, P. Pattnaik, and M. L. Klein. 1998. The M2 channel of influenza A virus: a molecular dynamics study. *FEBS Lett.* 434:265–271.

49. Case, D. A., D. A. Pearlman, J. W. Caldwell, T. E. Cheatham, III, J. Wang, W. S. Ross, C. L. Simmerling, T. A. Darden, K. M. Merz, R. V. Stanton, A. L. Cheng, J. J. Vincent, et al. (2002). AMBER 7. University of California, San Francisco, CA.

50. Aqvist, J. 1990. Ion-water interaction potentials derived from free energy perturbation simulations. *J. Phys. Chem.* 94:8021–8024.

51. Cornell, W. D., P. Cieplak, C. I. Bayly, I. R. Gould, K. M. Merz, Jr., D. M. Ferguson, D. C. Spellmeyer, T. Fox, J. W. Caldwell, and P. A. Kollman. 1995. A second-generation force field for the simulation of proteins and nucleic acids. *J. Chem. Phys.* 117:5179–5197.

52. Jorgensen, W. L., J. D. Chandrasekhar, J. D. Madura, R. W. Impey, and M. L. Klein. 1983. Comparison of simple potential functions for simulating liquid water. *J. Chem. Phys.* 79:926–935.

53. Kaminski, G., E. Duffy, T. Matsui, and W. L. Jorgensen. 1994. Free energies of hydration and pure liquid properties of hydrocarbons from the OPLS all-atom model. *J. Phys. Chem.* 98:13077–13082.

54. Chen, B., M. Martin, and J. Siepmann. 1998. Thermodynamic properties of the Williams, OPLS-AA, and MMFF94 all-atom force fields for normal alkanes. *J. Phys. Chem. B.* 102:2578–2586.

55. Ryckaert, J. P., G. Ciccotti, and H. J. C. Berendsen. 1977. Numerical integration of the Cartesian equations of motion of a system with constraints: molecular dynamics of n-alkanes. *J. Comput. Phys.* 23: 327–341.

56. Essman, U., L. Perera, M. L. Berkowitz, T. Darden, H. Lee, and L. G. Pedersen. 1995. A smooth particle mesh Ewald method. *J. Chem. Phys.* 103:8577–8593.

57. van Gunsteren, W. F., and H. J. Berendsen. 1984. Computer simulation as a tool for tracing the conformational differences between proteins in solution and in the crystalline state. *J. Mol. Biol.* 176:559–564.

58. Xue, T., and A. Li. 2002. An external determinant in the S5-P linker of the pacemaker (HCN) channel identified by sulfhydryl modification. *J. Biol. Chem.* 227:46233–46242.

59. Rothberg, B. S., K. S. Shin, and G. Yellen. 2003. Movements near the gate of a hyperpolarization-activated cation channel. *J. Gen. Physiol.* 122:501–510.

60. Ermler, U., W. Grabarse, S. Shima, M. Goubeaud, and R. Thauer. 1998. Active sites of transition metals enzymes with a focus on nickel. *Curr. Opin. Struct. Biol.* 8:749–758.

61. Maroney, M. 1999. Structure/function relationships in nickel metallobiochemistry. *Curr. Opin. Chem. Biol.* 3:188–199.

62. Srinivasan, N., R. Sowdhamini, C. Ramakrishnan, and P. Balaram. 1989. Conformations of disulfide bridges in proteins. *Int. J. Pept. Res.* 36:147–155.

63. Glusker, J. 1991. Structural aspects of metal liganding to functional groups in proteins. *Adv. Protein Chem.* 42:1–76.

64. Johnson, J., and W. N. Zagotta. 2001. Rotation movement during cyclic nucleotide-gated channel opening. *Nature.* 412:917–921.

65. Careaga, C., and J. Falke. 1992. Thermal motions of surface alpha-helices in the D-galactose chemosensory receptor. *J. Mol. Biol.* 226: 1219–1235.

66. Furey, W. F., A. H. Robbins, L. L. Clancy, D. R. Winge, B. C. Wang, and C. D. Stout. 1986. Crystal structure of Cd,Zn metallothionein. *Science.* 231:704–710.

67. Changela, A., K. Chen, Y. Xue, J. Holschen, C. E. Outten, T. V. O'Halloran, and A. Mondragon. 2003. Molecular basis of metal-ion selectivity and zeptomolar sensitivity by CueR. *Science.* 301:1383–1387.

68. Domene, C., and M. S. Sansom. 2003. Potassium channel, ions, and water: simulation studies based on the high-resolution x-ray structure of KcsA. *Biophys. J.* 85:2787–2800.

69. Zhou, M., and R. MacKinnon. 2004. A mutant KcsA K(+) channel with altered conduction properties and selectivity filter ion distribution. *J. Mol. Biol.* 338:839–846.

70. Choi, H., and L. Heginbotham. 2004. Functional influence of the pore helix glutamate in the KcsA K+ channel. *Biophys. J.* 86:2137–2144.

71. Becchetti, A., K. Gamel, and V. Torre. 1999. Cyclic nucleotide-gated channels. Pore topology studied through the accessibility of reporter cysteines. *J. Gen. Physiol.* 114:377–392.

72. Liu, J., and S. A. Siegelbaum. 2000. Change of pore helix conformational state upon opening of cyclic nucleotide-gated channels. *Neuron.* 28:899–909.

73. Flynn, G. E., and W. N. Zagotta. 2001. Conformational changes in S6 coupled to the opening of cyclic nucleotide-gated channels. *Neuron.* 30:689–698.

74. Guidoni, L., V. Torre, and P. Carloni. 2000. Water and potassium dynamics inside the KcsA K(+) channel. *FEBS Lett.* 477:37–42.

75. Allen, T. W., O. S. Andersen, and B. Roux. 2004. On the importance of atomic fluctuations, protein flexibility, and solvent in ion permeation. *J. Gen. Physiol.* 124:679–690.